



Published in final edited form as:

IEEE Sens Lett. 2021 November ; 5(11): . doi:10.1109/lensens.2021.3122097.

A High Sensitivity Transparent Ultrasound Transducer based on PMN-PT for Ultrasound and Photoacoustic Imaging

Haoyang Chen¹ [Student Member, IEEE],

Shubham Mirg¹,

Mohamed Osman¹,

Sumit Agrawal¹,

Jiacheng Cai¹,

Ryan Biskowitz¹,

Josiah Minotto¹,

Sri-Rajasekhar Kothapalli^{1,2,3} [Member, IEEE]

¹Department of Biomedical Engineering, The Pennsylvania State University, State College, PA, 16802, USA

²Penn State Cancer Institute, The Pennsylvania State University, Hershey, PA, 17033, USA

³Graduate Program in Acoustics, The Pennsylvania State University, State College, PA 16802, USA

Abstract

We recently introduced piezoelectric lithium niobate (LN) based transparent ultrasound transducers (TUT) as a new platform for developing multimodal optical, ultrasound and photoacoustic imaging systems. However, LN based TUT is limited in its signal-to-noise ratio due to material's low piezoelectricity (d_{33}). In this paper, we report, for the first time, a 0.2 mm thick transparent lead magnesium niobate-lead titanate (PMN-PT) based TUT (PMN-PT-TUT) for ultrasound and photoacoustic applications and compared its performance with a 0.25 mm thick transparent LN based TUT (LN-TUT). To improve the ultrasound energy transmission efficiency, TUTs were fabricated with a two-matching-layer design. This resulted in a dual frequency response with center frequencies of 7.8 MHz/13.2 MHz and corresponding bandwidths of 28.2%/66.67% for PMN-PT-TUT, and center frequencies of 7.2 MHz/11.8 MHz and bandwidths of 36.1%/62.7% for LN-TUT. The optical transmission rate of PMN-PT-TUTs and LN-TUTs are measured as ~73% and ~91% respectively at 532 nm optical wavelength. The PMN-PT-TUT exhibited higher sensitivity compared to LN-TUT with a nearly three-fold higher pulse echo amplitude and more than two-fold higher photoacoustic amplitude. Furthermore, optical resolution photoacoustic microscopy (ORPAM) experiments on phantom targets demonstrated lateral resolutions of 7 μm and 5.1 μm , and axial resolutions of 285.6 μm and 375.9 μm for PMN-PT-TUT and LN-TUT respectively. These results indicated that PMN-PT is a viable alternative to LN for developing TUT based multimodal ultrasound and photoacoustic imaging systems.

Corresponding author: Sri-Rajasekhar Kothapalli (srkothapalli@psu.edu).
Haoyang Chen and Shubham Mirg are co-first authors.

Keywords

Photoacoustic imaging; photoacoustic microscopy; PMN-PT; transparent ultrasound transducers

I. INTRODUCTION

Recent advances in transparent ultrasound transducers (TUT) have enabled a new platform for developing multimodal imaging combining optical, ultrasound, and photoacoustic technologies [1]-[3]. Conventional ultrasound imaging as well as photoacoustic imaging (PAI) employ ultrasound transducers that are opaque to light, therefore hindering coaxial alignment. This in turn leads to near field shadowing in PAI and necessitates a considerably large standoff distance (~ 1 cm) between the transducer head and the tissue medium. The standoff region is filled with water or ultrasound gel to allow ultrasound wave coupling. Such a large unwanted coupling medium brings discomfort to the living subjects being imaged, introduces artifacts, and precludes longitudinal scanning and ultrafast imaging [4], [5]. By allowing optical illumination through the transducer, TUTs, not only can overcome the above-mentioned problems and considerably simplify the PAI imaging head, but also provide an elegant platform for integrating multiple synergistic imaging and ultrasound stimulation approaches.

In PAI, a non-ionizing laser pulse illuminates the tissue, and the light-absorbing chromophores in the tissue generate heat, causing marginal expansion followed by their rapid cooling. This induces broadband acoustic waves which are then captured by the ultrasonic transducer as a function of incident optical wavelength to extract quantitative spectral PAI information about the chromophores. Conventional ultrasound transducers are opaque and therefore require optical illumination to circumnavigate the transducer by mechanisms such as acoustic optic combiners, angled illumination or ring transducers [5] which not only increases cost and complexity of the setup but also prevents miniaturization. Thus, TUTs are much needed to allow for coaxial illumination of the optical beam through the transducer. All optical ultrasound detectors, such as Fabry-Perot etalons and micro ring resonators, are also transparent to light and exhibit high PAI sensitivity for smaller areas. However, they require additional lasers for operation, lack ultrasound transduction/stimulation capabilities, and need complex fiber integration [6]. To address the above limitations, we earlier developed and demonstrated lithium niobate (LN) based TUTs (LN-TUT) for general PAI [1] as well as optical resolution photoacoustic microscopy (ORPAM) [7]. Recently several research groups have adapted the LN-TUT technology for different PAI applications [8], including focused TUT [3] and large field-of-view ORPAM [9]. While all these studies established the potential of TUTs for PAI, the PA signal detection sensitivity is not as high as conventional ORPAM that is shown to image single red blood cell oxygenation inside the microvasculature [10]. This can be partly attributed to the low piezoelectricity (d_{33}) of LN that leads to low electromechanical coupling coefficient (k_{eff}) and PAI sensitivity. Novel transparent piezoelectric materials with higher d_{33} and k_{eff} can potentially improve the overall ultrasound and photoacoustic sensitivity. Qiu et. al. recently reported that by alternating current (AC) poling, lead magnesium niobate-lead titanate (PMN-PT) could be made transparent with ultrahigh piezoelectricity [11]. Based

on this material advance, we developed LN and PMN-PT based TUTs using our recently reported two-matching-layer design [12] and compared their performance using electrical, acoustic and photoacoustic measurements. In comparison to LN-TUT, PMN-PT based TUT (PMN-PT-TUT) showed three times improved ultrasound pulse echo amplitude, twice the photoacoustic amplitude, broader bandwidth, and obtained sharply resolved high contrast photoacoustic microscopy images.

II. MATERIALS AND METHODS

A. Design and Fabrication of TUT

In contrast to earlier TUTs that use only Parylene C as a matching layer [8], [12], here we introduce a two-matching-layer design to greatly enhance the ultrasound transmission efficiency of TUTs, fabricated using the two transparent piezoelectric materials of interest: PMN-28PT (X2A, TRS Technologies, State College, PA, USA) and LN (Precision Micro Optics, Burlington, MA, USA). The design parameters for the TUTs are summarized in the Table 1. These parameters were optimized using a transducer modeling software (PiezoCAD, Sonic Concepts, Woodinville, WA, USA). The fabrication process was as follows: 1) A 200 nm thick indium tin oxide (ITO) was first sputtered on both sides of the piezoelectric material to serve as transparent conductive electrodes. 2) The piezoelectric material was diced into square shapes ($3\times 3\text{ mm}^2$) and then pressed to bond with the first matching layer - a quarter-wavelength thick micro glass slide ($\sim 100\ \mu\text{m}$) - using a small amount of transparent epoxy (EPO-TEK 301, Epoxy Technologies Inc., Billerica, MA, USA) as the bonding agent. 3) A square brass tube with 2 mm height was used as the outer housing and filled with the transparent epoxy as the backing layer. 4) Then the brass tube was connected to the front ITO electrode of the piezoelectric material using a silver epoxy (E-solder 3022, Von Roll Isola Inc., New Haven, CT, USA). 5) In the final step, a quarter-wavelength thick ($\sim 40\ \mu\text{m}$) Parylene-C film was coated on the transducer to serve as a protective and biocompatible second matching layer.

In order to ease the transducer fabrication process due to the low Curie temperature characteristic of PMN-PT ($80\text{ }^\circ\text{C}$ from TRS data sheet), the PMN-PT-TUTs were poled after the assembly of the transducer layers. According to Qiu et. al [11] and our previous observation [12], AC poled PMN-28PTs exhibited higher optical transmission than the corresponding DC poled PMN-28PTs. Therefore, PMN-PT-TUTs were AC poled using 30 cycles of 1 Hz triangular wave with an electric field of 3.5 kV/cm. On the other hand, LN-TUTs did not need re-poling as they exhibit high Curie temperature ($1150\text{ }^\circ\text{C}$ [13]) and would not be easily depoled during the fabrication process. LN-TUT and AC-poled PMN-PT-TUT are shown in Fig. 1a and 1b (sizes of $6\times 6\text{ mm}^2$ are shown for better clarity). The picture of the Nittany Lion Mascot can be seen clearly through both the TUTs without optical distortion.

B. Electrical, Acoustic, and Optical Characterization

The optical transmission of fabricated TUTs was first evaluated at 532 nm as well as in near-infrared (NIR) spectrum from 690 nm to 960 nm (with a 20 nm interval) by determining the optical energy difference from a tunable laser (Phocus Mobile, Oportek Inc.,

Carlsbad, CA, USA) before and after passing through the TUT, measured by a pyroelectric energy meter (PE50BF-DIFH-C, Ophir-Spiricon, LLC, North Logan, UT, USA). Thereafter, the TUTs were characterized by electrical impedance analyzer (Agilent E5100A, Keysight Technologies, Inc., Santa Rosa, CA, USA) for determining the resonance and anti-resonance frequencies, and thereby calculating the k_{eff} . As described in our previous work [7], the two-way ultrasound pulse-echo response and corresponding frequency characteristics of TUTs were measured using the ultrasound pulser receiver (Olympus 5073PR, Olympus NDT Inc., Waltham, MA, USA).

C. Optical Resolution Photoacoustic microscopy

The ORPAM performance of PMN-PT- and LN-TUTs are studied using an experimental setup similar to our previous work [7], with the following minor modifications: an objective lens of 75 mm focal length (AC254-075-A, Thorlabs, Newton, NJ, USA) was used for light focusing, and photoacoustic signals were filtered using a 3-30 MHz RF bandpass filter (ZABP-16+, Mini-Circuits, Branson, MO, USA) followed by amplification using two 28 dB amplifiers (ZFL-500LN+, Mini-Circuits, Branson, MO, USA) in series. The incident laser light (GLPM-10, IPG Photonics, Oxford, MA, USA) had a repetition rate of 10 kHz, 1.4 ns pulse width and 0.5 μJ pulse energy right before passing through the TUT. ORPAM scans of USAF resolution-test target and a 7-9 μm carbon fiber phantom were performed at 64 averages using both PMN-PT- and LN-TUTs. These measurements were used to calculate the spatial resolution, photoacoustic bandwidth, and SNR for both TUTs.

III. RESULTS AND DISCUSSION

We first studied the optical transmittance of both LN-TUT and PMN-PT-TUT at 532 nm wavelength and also in the NIR wavelength regions. At 532 nm wavelength, the transmittance values were calculated to be $91.09\% \pm 1.56\%$ for LN-TUT and $73.15\% \pm 0.79\%$ for PMN-PT-TUT. In the NIR spectrum, LN-TUT showed an optical transmittance of $> 80\%$ whereas PMN-PT-TUT showed $> 70\%$ transmittance, as shown in Fig. 1c. Table 2 summarizes the comparison of electrical impedance, pulse-echo, and ORPAM results for PMN-PT- and LN-TUTs (the parameter that outperformed the other was bolded in text). First, they were compared by their electrical properties. Figs. 2a and 2b show the simulated and experimentally measured electrical input impedances for the two-matching-layer PMN-PT-TUT fabrication discussed above. The impedance difference between the simulation and measurements can be a result of the sheet resistance of deposited ITO that could not be factored in PiezoCAD. The phase difference can be contributed by a small amount of residual bonding agent in between the glass matching layer and the piezoelectric material. The simulated and measured impedance curves for two-matching-layer LN-TUTs are not shown, but can be found in our recent work [12]. These results show that LN-TUT has resonance and anti-resonance frequencies as 14.30 MHz and 15.43 MHz respectively at 400 Ω in comparison to PMN-PT-TUT has resonance and anti-resonance frequencies as 11.66 MHz and 16.37 MHz respectively at 60 Ω . From these frequency values, the k_{eff} for LN- and PMN-PT-TUTs were calculated to be 0.376 and 0.655 respectively, indicating PMN-PT has a better transduction efficiency and making it a more suitable material for ultrasound transducer. Next we characterized the two-way ultrasound pulse echo for both TUTs using

a flat metal target kept at ~ 25 mm away from the transducers in deionized water medium. Due to the glass matching slide, both TUTs exhibited a dual frequency nature, and the measured center frequencies for LN- and PMN-PT-TUTs were 7.2 MHz/11.8 MHz and 7.8 MHz/13.2 MHz respectively (Figs. 2d and 2f), which matched well with their simulated pulse echo response (Figs. 2c and 2e). The corresponding -6 dB pulse echo bandwidths were measured to be: 36.1%/62.7% and 28.2%/66.67% for LN and PMN-PT respectively. Compared to the earlier TUTs with only one matching layer [8], [9], the two-matching-layer TUTs reported here showed a broader frequency response. When comparing the pulse echo amplitudes, PMN-PT-TUT (1.64 V) outperformed LN-TUT (0.62 V) by nearly three-fold and corresponding SNR values by 8.9 dB (53.7 dB vs 44.8 dB). This agreed well with the observed electrical impedance measurements and simulated pulse echo responses.

Next, we studied the photoacoustic sensitivity of the PMN-PT-TUT and LN-TUT using ORPAM experiments. First we compared the photoacoustic A-line response from a carbon fiber ($7 - 9 \mu\text{m}$ thick) phantom. Similar to the pulse echo response, PMN-PT-TUT obtained a higher - more than two-fold - photoacoustic amplitude than that of LN (1.33 V versus 0.68 V in Figs. 3a and 3b). The signal-to-noise ratio (SNR) was calculated by the $20\log_{10}$ ratio of the peak-to-peak photoacoustic amplitude to the noise standard deviation and was found to be 43.7 dB and 48.9 dB for LN- and PMN-PT-TUTs respectively. The doubled PA amplitude was expected to yield a > 6 dB increase in SNR for PMN-PT-TUT compared to LN-TUT. However, the lower optical transmittance of PMN-PT due to increased optical absorption induced a thermoacoustic noise inside the material. Despite this, the photoacoustic SNR from the two-matching layer PMN-PT-TUT is nearly 5 dB higher than that of LN-TUT; and nearly 11 dB higher than our previous no-matching layer LN-TUT (38 dB) [7]. The -6 dB bandwidths derived from frequency response of the photoacoustic A-lines for two TUTs were calculated to be 50%/72.3% for LN and 55.3%/78.3% for PMN-PT (Figs. 3a and 3b). By taking the envelope of the photoacoustic A-line signal, the axial resolutions were then measured to be $375.9 \mu\text{m}$ for LN and $285.6 \mu\text{m}$ for PMN-PT. These reduced axial resolutions compared to our previously reported no-matching layer LN-TUT axial resolution ($150 \mu\text{m}$) [7], can be attributed to the low frequency component (~ 7 MHz) introduced by the two-matching-layer TUTs that broadened the pulse length.

While studying the ORPAM capabilities of PMN-PT- and LN-TUTs, we first characterized the lateral resolution by edge scanning of a USAF resolution target. Figs. 3c and 3d show the obtained edge spread functions (ESFs) along the red dashed line of the figure insets for LN and PMN-PT-TUT, respectively. Also shown in each of these figures are the line spread functions (LSFs) obtained by the derivative of respective ESFs. The lateral resolutions, defined as the full-width-half-maxima (FWHM) of the LSF, were calculated to be $5.1 \mu\text{m}$ for LN-TUT and $7 \mu\text{m}$ for PMN-PT TUT. The slightly reduced lateral resolution for PMN-PT-TUT, observed in all our experiments, could be due to small scale optical aberrations induced by PMN-PTs.

Parameters	Lithium Niobate	AC-Poled PMN-PT
d_{33} (pC N ⁻¹)	350 pC N ⁻¹	2200 pC N⁻¹
Resonance Frequency (measured)	14.3 MHz	11.66 MHz
Anti-resonance Frequency (measured)	15.43 MHz	16.37 MHz
k_{eff}	0.376	0.655
Pulse Echo Amplitude	0.62 V	1.64 V
Pulse Echo SNR	44.8 dB	53.7 dB
Center Frequency (measured)	7.2 MHz/11.8 MHz	7.8 MHz/13.2 MHz
-6 dB Bandwidth (measured)	36.1%/62.7%	28.2%/ 66.67%
Optical Transmission at 532 nm	91.09% ± 1.56%	73.15% ± 0.79%
Photoacoustic Amplitude	0.678 V	1.329 V
Photoacoustic SNR	43.7 dB	48.9 dB
-6 dB Photoacoustic Bandwidth	50%/72.3%	55.3%/78.3%
PAM axial resolution	375.9 μm	285.6 μm
PAM lateral resolution	5.1 μm	7 μm

d_{33} : piezoelectricity coefficient; k_{eff} : effective electromechanical coupling coefficient; SNR: signal-to-noise ratio; PAM: photoacoustic microscopy.

Lastly, we demonstrated the first use, to the best of our knowledge, of the highly sensitive AC poled PMN-PT-TUT for photoacoustic microscopy imaging by scanning across a 7-9 μm carbon fiber phantom. Fig. 3e shows the corresponding maximum amplitude projection (MAP) image of the phantom obtained from processing the peak to peak values of the photoacoustic signals during the raster scanning. A B-scan image in Fig. 3f, obtained across the white dashed line shown in Fig 3e, clearly shows the depth of the fibers inside the agar phantom.

In conclusion, we reported a high sensitivity AC poled PMN-PT-TUT using two-matching-layer design and compared its performance with LN-TUT. PMN-PT-TUTs outperformed the LN-TUTs with a three-fold higher pulse echo amplitude, 8.9 dB higher SNR in ultrasound pulse-echo, a two-fold higher photoacoustic amplitude, and 5 dB higher photoacoustic SNR. While PMN-PT-TUT exhibited higher axial resolution and bandwidths due to improved piezoelectric properties of the PMN-PT material, the lateral resolution of LN-TUT was slightly tighter due to better optical properties. The sharply resolved carbon fiber phantom image showed that the AC poled PMN-PT can be a preferable alternative to LN for TUT based wearable and multimodal imaging applications with ultrasound stimulation capabilities. Moreover, in the future, computational approaches [14], [15] can help improve the photoacoustic SNR of the TUTs.

ACKNOWLEDGMENT

We acknowledge Eugene Gerber for support in the machining of parts and help with transducer design. We also thank Christopher Cheng for help in Parylene coating.

This research was funded by NIH-NIBIB R00EB017729-05 (SRK), the Penn State Cancer Institute—Highmark seed grant (SRK), College of Engineering multidisciplinary grant, and Grace Woodward grant (SRK).

REFERENCES

- [1]. Dangi A et al. , “Lithium niobate-based transparent ultrasound transducers for photoacoustic imaging,” *Opt. Lett.*, vol. 44, no. 21, pp. 5326–5329, Nov 2019. [PubMed: 31674999]
- [2]. Ilkhechi AK et al. , “Transparent capacitive micromachined ultrasonic transducer (cmut) arrays for real-time photoacoustic applications,” *Optics express*, vol. 28, no. 9, pp. 13 750–13 760, 2020.
- [3]. Park S et al. , “Optically transparent focused transducers for combined photoacoustic and ultrasound microscopy,” *Journal of Medical and Biological Engineering*, vol. 40, pp. 707–718, 2020.
- [4]. Wells PNT, “Ultrasound imaging,” *Physics in Medicine and Biology*, vol. 51, no. 13, pp. R83–R98, jun 2006. [PubMed: 16790922]
- [5]. Li L et al., *Photoacoustic Tomography of Neural Systems*. Cham: Springer International Publishing, 2020, pp. 349–378.
- [6]. Dong B et al. , “Optical detection of ultrasound in photoacoustic imaging,” *IEEE Transactions on Biomedical Engineering*, vol. 64, no. 1, pp. 4–15, 2016. [PubMed: 27608445]
- [7]. Chen H et al. , “Optical-resolution photoacoustic microscopy using transparent ultrasound transducer,” *Sensors*, vol. 19, no. 24, 2019.
- [8]. Chen R et al. , “Transparent high-frequency ultrasonic transducer for photoacoustic microscopy application,” *IEEE transactions on ultrasonics, ferroelectrics, and frequency control*, vol. 67, no. 9, pp. 1848–1853, 2020. [PubMed: 32286968]
- [9]. Liao T et al. , “Centimeter-scale wide-field-of-view laser-scanning photoacoustic microscopy for subcutaneous microvasculature in vivo,” *Biomed. Opt. Express*, vol. 12, no. 5, pp. 2996–3007, May 2021. [PubMed: 34168911]
- [10]. Wang L et al. , “Single-cell label-free photoacoustic flowoxigraphy in vivo,” *Proceedings of the National Academy of Sciences*, vol. 110, no. 15, pp. 5759–5764, 2013.
- [11]. Qiu C et al. , “Transparent ferroelectric crystals with ultrahigh piezoelectricity,” *Nature*, vol. 577, no. 7790, pp. 350–354, Jan 2020. [PubMed: 31942055]
- [12]. Chen H et al., “Transparent ultrasound transducers for multiscale photoacoustic imaging,” in *Photons Plus Ultrasound: Imaging and Sensing 2021*, vol. 11642, International Society for Optics and Photonics. SPIE, 2021, pp. 142 – 149.
- [13]. Fei C et al. , “Ultrahigh frequency (100 mhz–300 mhz) ultrasonic transducers for optical resolution medical imaging,” *Scientific reports*, vol. 6, no. 1, pp. 1–8, 2016. [PubMed: 28442746]
- [14]. Hariri A et al. , “Deep learning improves contrast in low-fluence photoacoustic imaging,” *Biomed. Opt. Express*, vol. 11, no. 6, pp. 3360–3373, Jun 2020. [PubMed: 32637260]
- [15]. Johnstonbaugh K et al. , “A Deep Learning Approach to Photoacoustic Wavefront Localization in Deep-Tissue Medium,” *IEEE Trans. Ultrason. Ferroelectr. Freq. Control*, vol. 67, no. 12, pp. 2649–2659, Jan 2020. [PubMed: 31944951]

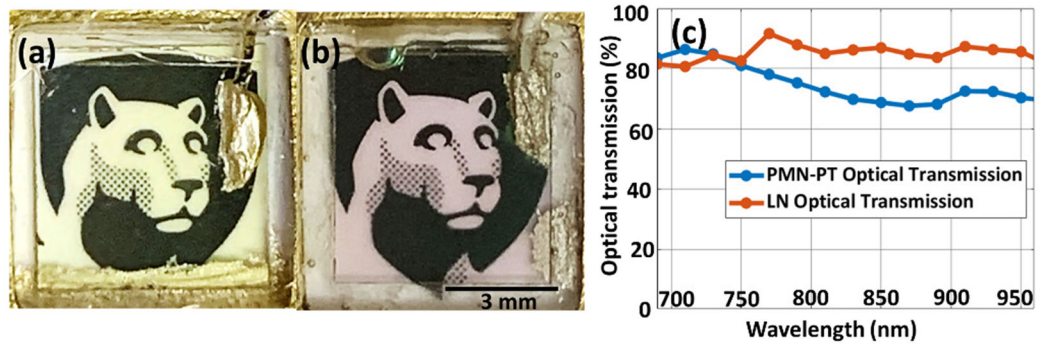


Fig. 1. Pictures of fabricated optically transparent (a) LN and (b) PMN-PT based transparent ultrasound transducers (TUT) on top of a black and white Nittany Lion mascot image. (c) shows the optical transmission comparison plot between LN- (red) and PMN-PT- (blue) TUTs in near-infrared spectrum.

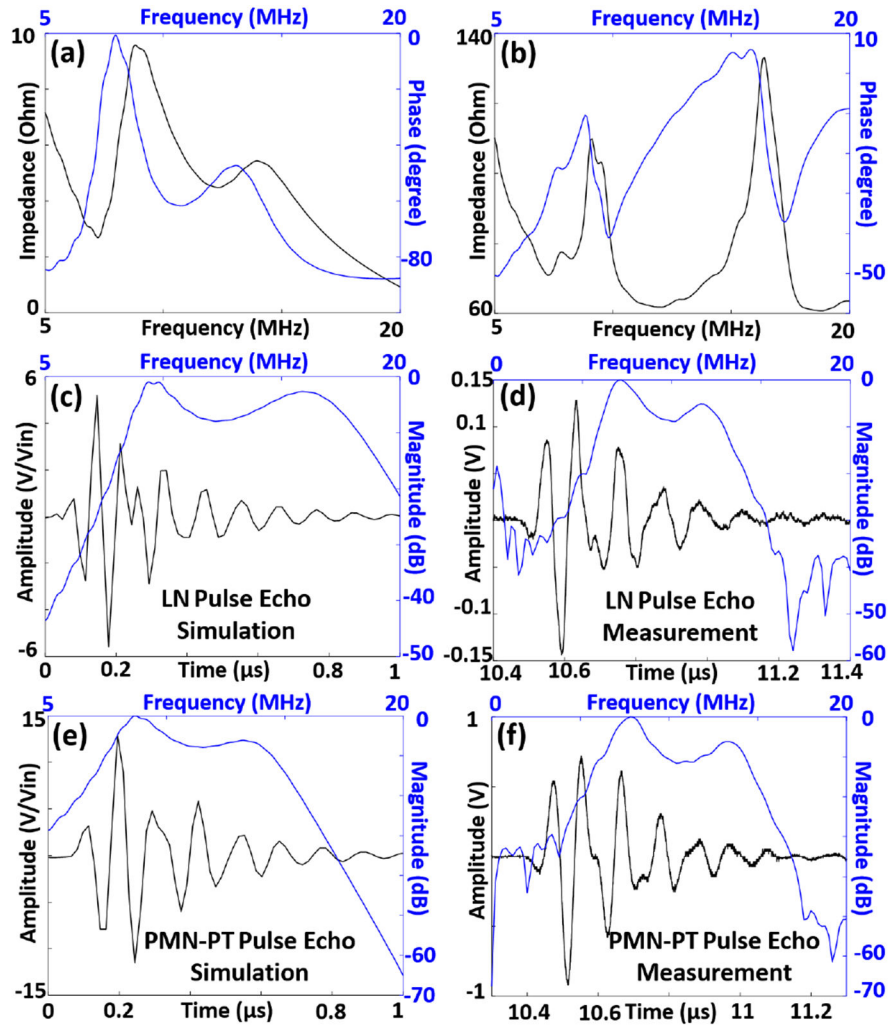


Fig. 2. The simulated and measured transducer characterization results: (a) Simulated and (b) experimental electrical input impedance measurements for the PMN-PT transparent ultrasound transducer, black line represents the impedance curve, and the blue line represents the phase curve. Two way ultrasound pulse echo responses for (c) simulated and (d) experimental LN-TUT; and (e) simulated and (f) experimental PMN-PT-TUT. Black line represents the time domain signal, and the blue line represents the corresponding frequency response.

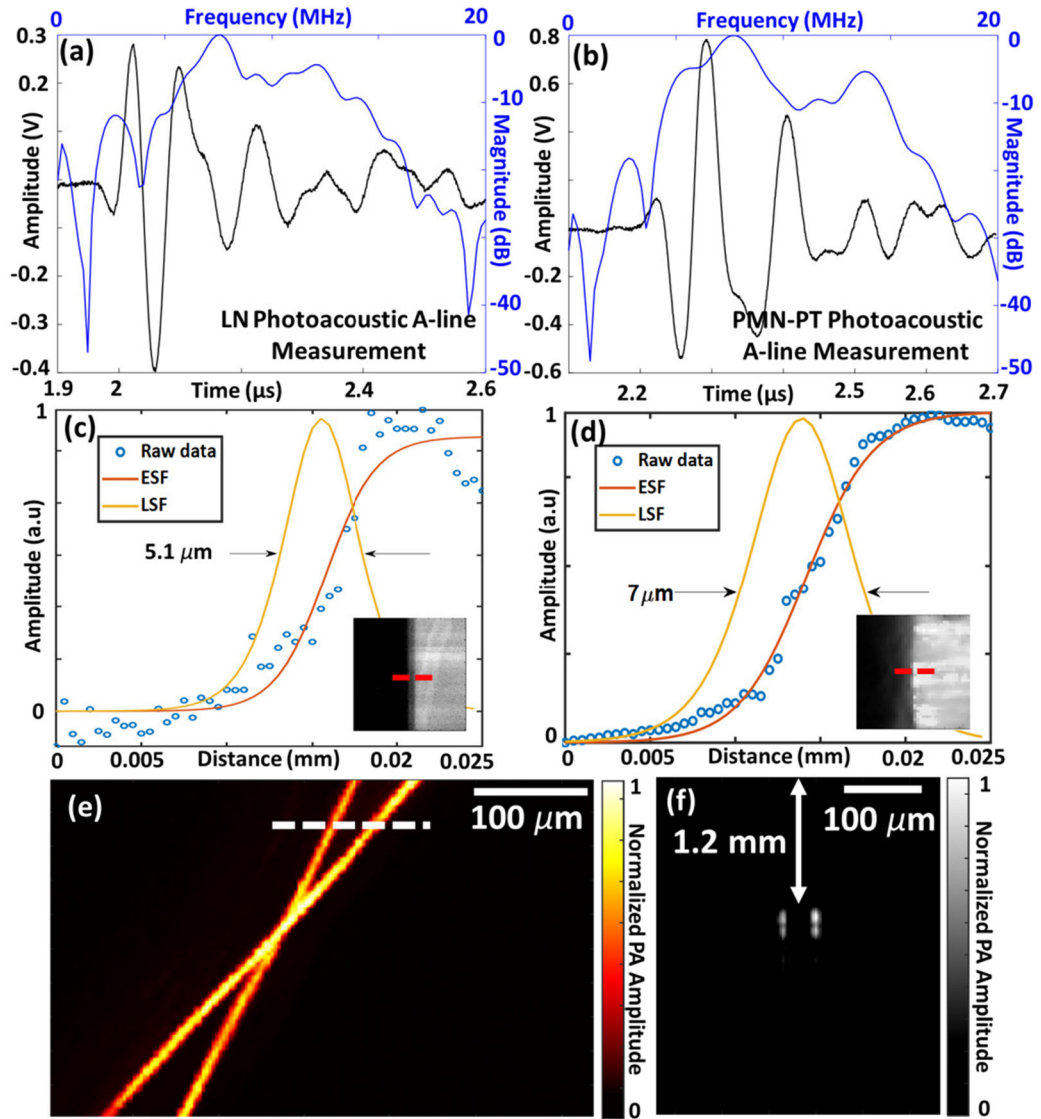


Fig. 3. Photoacoustic microscopy imaging results: photoacoustic A-line responses for (a) lithium niobate and (b) PMN-PT based transparent ultrasound transducers. The black line represents the time domain signal and blue line represents the corresponding frequency response. Lateral resolution measurement from the edge of a USAF target for (c) lithium niobate and (d) PMN-PT using fitted edge spread function (ESF) and line spread function (LSF). Insets show scanned images with the red dashed line indicating the scanning line for ESF. (e) Photoacoustic maximum amplitude projection (MAP) image of a carbon fiber phantom, and (f) a B-scan photoacoustic image along the white dashed line in (e).

TABLE 1.

Design Parameters for Transparent Ultrasound Transducer.

Specifications	Values
Center Frequency	13 MHz
Thickness of Piezoelectric Material	200 μm (PMN-28PT) and 250 μm (LN)
Thickness of Backing Layer	2 mm
Thickness of Matching Layer 1	100 μm
Thickness of Matching Layer 2	40 μm

Author Manuscript

Author Manuscript

Author Manuscript

Author Manuscript